Journal of Power Sources 252 (2014) 122–129

Contents lists available at ScienceDirect

Journal of Power Sources

journal homepage: www.elsevier.com/locate/jpowsour

Preparation and performances of Co–Mn spinel coating on a ferritic stainless steel interconnect material for solid oxide fuel cell application

H.H. Zhang, C.L. Zeng*

State Key Laboratory for Corrosion and Protection, Institute of Metal Research, Chinese Academy of Science, 62 Wencui Road, Shenyang 110016, China

HIGHLIGHTS

- Co–Mn alloys are deposited in chloride solutions to protect metallic interconnects.
- The Co–Mn alloy is converted into adhesive spinel coatings by heat treatment in air.
- Spinel coatings consist of an external $MnCo_2O_4$ layer and an inner Cr-rich layer.
- spinel coatings inhibit the oxidation of the steel at 800 °C in air and air-10%H_2O.
- Spinel coatings decrease the area specific electrical resistance of the steel.

ARTICLE INFO

Article history:
Received 14 September 2013
Received in revised form
7 November 2013
Accepted 2 December 2013
Available online 11 December 2013

Keywords:
Solid oxide fuel cell
Interconnect
Electrodeposition
Spinel coating
Oxidation
Area specific electric resistance

ABSTRACT

Ferritic stainless steels have become the candidate materials for interconnects of intermediate temperature solid oxide fuel cell (SOFC). The present issues to be solved urgently for the application of ferritic stainless steel interconnects are their rapid increase in contact resistance and Cr poisoning. In the present study, a chloride electrolyte suspension has been developed to electro-deposit a Co–Mn alloy on a type 430 stainless steel, followed by heat treatment at 750 °C in argon and at 800 °C in air to obtain Co–Mn spinel coatings. The experimental results indicate that an adhesive and compact Co–Mn alloy layer can be deposited in the chloride solution. After heat treatment, a complex coating composed of an external $MnCo_2O_4$ layer and an inner Cr-rich oxide layer has been formed on 430SS. The coating improves the oxidation resistance of the steel at 800 °C in air, especially in wet air, and inhibits the outward diffusion of Cr from the Cr-rich scale. Moreover, a low contact resistance has been achieved with the application of the spinel coatings.

1. Introduction

Solid oxide fuel cell (SOFC) is a promising candidate for energy conversion due to its advantages of high efficiency and reduced emissions over the traditional energy-conversion systems. The progress in the fabrication technology of SOFCs has made it possible to reduce the operating temperature of cells from the initial 1000 °C to the intermediate-temperature range of 600–800 °C without compromising the performance [1–3]. In consequence, some relatively cheap Cr_2O_3-forming alloys such as ferritic stainless steels could be used as interconnects in replacement of expensive ceramics [4–8].

In addition to feasible and low-cost fabrication of interconnects, metals also have excellent thermal and electrical conductivity in comparison with ceramics. The main obstacles for the application of chromia-forming alloy interconnects are the fast increase of area specific resistance (ASR) induced by the oxidation of metallic interconnects and the poisoning of the porous cathode caused by volatile Cr species from the chromia scale [9–12]. Several technologies including alloy bulk composition modifications, surface treatments and protective coatings have been attempted to overcome these problems. Among these approaches, applying protective and electrically conductive coatings is a simple and effective method. Up to now, various coating materials have been investigated in an attempt to decrease the growth of oxide scales and inhibit the volatilization of Cr species from the Cr-rich scales while maintaining a low ASR. The state-of-art coating materials mainly include reactive element oxides [13,14], conductive perovskites [15,16], MAlCrYO(M represents a metal such as Co, Mn, and/or Ti)

* Corresponding author. Tel.: +86 24 23904553; fax: +86 24 23893624.
E-mail address: clzeng@imr.ac.cn (C.L. Zeng).

0378-7753/$ – see front matter © 2013 Elsevier B.V. All rights reserved.
http://dx.doi.org/10.1016/j.jpowsour.2013.12.007

oxidation resistant systems [17,18], conductive spinels [19–22] and conductive composite spinels [23,24], among which conductive perovskites and spinels have attracted significant attention. Recently, Shaigan et al. [25] and Wu et al. [26] presented a comprehensive review of progresses in coatings, surface modifications and alloy developments for the metallic interconnects of SOFC, respectively.

In addition to the advantages of good electrical conductivity and thermal compatibility, rare earth perovskite coatings may decrease the oxidation rate and improve the scale adhesion by supplying reactive elements to the underlying thermally grown oxide scale. However, perovskites are unsuitable for protective purposes due to the fact that they are ionically conductive in nature and may transport oxygen ions, and thus their coatings cannot substantially inhibit Cr migration or absorb migrating Cr species [25]. When lanthanum chromite ($LaCrO_3$) is exposed directly to the wet air, it still releases volatile Cr species, although at a rate three orders of magnitude lower than that for Cr_2O_3(s), leading to an unaccepted degradation in cell performances [27,28].

Recently, spinel coatings have received wide attention due to their advantages of good electrical conductivity, excellent coefficient of thermal expansion (CTE) match with the ferritic stainless steel substrate and other cell components such as anode and cathode, and high capability for absorbing Cr species that migrate from the Cr_2O_3-rich scale to the scale surface [25]. Slurry [29–31] and electrodeposition methods [22,32] have been the main techniques for preparing spinel coatings on stainless steel substrate. Slurry coating processes mainly including spraying [29], screen printing [30] and plasma spraying [31] are simple and can produce thick coatings, but the coatings are usually porous and these techniques have limitations regarding homogenous layer thickness in the case of complex shaped interconnects. Electrodeposition of metal or alloy layers followed by oxidation treatment to obtain thermally-grown spinel layers on the steel substrates has been considered as an advantageous method for preparing spinel coatings. Electrodeposition method exhibits the advantages of better coating-substrate bonding, denser spinel layer and easier thickness control of spinel layer in comparison with slurry method.

Bateni et al. [31] prepared a dense and adhesive Co–Mn spinel coating on UNS 430 stainless steel by electrodepositing Co and Mn layers sequentially, followed by oxidation treatment at 750 °C in air. The coating showed good adhesion to the substrate during oxidation tests in air. However, the chemical composition is inhomogeneous in the coating along the depth direction. Direct electrodeposition of a Co–Mn alloy using direct current (DC) [33] or pulse plating [34] method has the potential to solve the chemical inhomogeneity within the spinel scale. Wu et al. [33] investigated DC co-deposition of Mn–Co alloys on stainless steels for SOFC interconnect application. The Mn–Co alloy coatings can be oxidized to be fully dense spinel coatings, which, however, are enriched in Mn, possibly due to the fast outward diffusion of Mn from the substrate. Pulse plating helps to improve the formation of alloys [34].

Mn has a very low reduction potential of $E_0(Mn^{2+}/Mn) = -1.42$ V vs. a saturated calomel electrode, which is the most electronegative metal that can be electrodeposited from aqueous solutions. Industrially, coatings made of manganese and its alloys are usually obtained by cathodic reduction of manganese sulphate and chloride together with corresponding ammonium salts [35]. Industrial electrodeposition of Co is usually conducted in sulphate electrolytes, with limited reports on chloride electrolytes [36]. The advantages of using chloride electrolytes with respect to sulphate include higher electrical conductivity in the electrolytes, lower overpotential for deposition of Co, lower anodic overpotential and higher cathodic current efficiency. The disadvantages of using chloride electrolytes are the generation of toxic anodic gas and higher stress.

In the present investigation, chloride electrolytes have been used to co-deposit dense and adhesive Co–Mn alloys in an attempt to prepare Co–Mn spinel coatings for ferritic stainless steel interconnects.

2. Experimental procedures

2.1. Preparation of Co–Mn spinel coatings

In this study, a type 430 stainless steel (430SS) was used as substrate alloy, whose chemical composition is Fe–17.0Cr–1.0Mn–1.0Si–0.12C–0.03S–0.04P (mass%). The steel plates were cut into sheet-shaped specimens with a size of 10 mm × 15 mm × 2 mm, followed by grinding with up to 600-grit SiC paper, sandblasting with an air-blast machine, and then cleaning with deionised water and ethanol, respectively. The specimens were pickled in 10% H_2SO_4 solution before electrodeposition.

Galvanostatic electrodeposition was carried out to produce a Co–Mn alloy layer on 430SS in a one-compartment cell using a two-electrode system with a graphite plate as the anode and 430SS as the cathode. The cathode was centred between two graphite plates. To decrease the deposition potential difference between Co and Mn and to promote the co-deposition of Co–Mn alloys, a novel chlorate electrolyte composed of 0.05 M $CoCl_2$, 1.25 M $MnCl_2$, 30 g L^{-1} NH_4Cl, 20 g L^{-1} NH_4Br and 0.05 M EDTA–Na_2 was used for electrodeposition. The addition of NH_4Br to the solution is aimed to inhibit the evolution of chlorine and oxygen on the graphite anode. The pH value of the solution was controlled to be 4.5. All solutions were prepared with analytical grade reagents and deionised water. The Co–Mn alloy coatings were optimally deposited on 430SS at a current density of 125 mA cm^{-2} for 0.5 h under ultrasonic agitation. After electrodeposition, the samples were treated at 750 °C for 2 h under the protection of high-purity argon, and then oxidized at 800 °C in air for 2 h to obtain thermally-grown Co–Mn spinel coatings.

2.2. Oxidation measurements

The oxidation of the uncoated and Co–Mn spinel-coated 430SS was conducted at 800 °C in air for 300 h and in wet air containing 10%H_2O for 100 h, respectively. The air oxidation was carried out in a high temperature muffle furnace. The samples were placed in alumina crucibles, and weighed after oxidation for various lengths of time. The wet air oxidation was conducted in a pit-type furnace with a quartz tube as the reaction chamber. Air was allowed to pass through a closed isothermal water box to produce wet air before flowing into the reaction chamber. The temperature of the water box was kept at 46 °C corresponding to 10% water vapour. The air flow rate was controlled to be 400 ml min^{-1}. When the furnace was heated to 800 °C, the reaction chamber was purged with wet air for 0.5 h before the specimen was moved into the reaction chamber for oxidation measurements. After oxidation for a certain time, the specimen was moved out of the furnace and then weighed.

2.3. Area specific electrical resistance measurements

The area specific electrical resistance (ASR) of the uncovered and covered steels was measured using a setup described elsewhere [37]. Platinum paste was applied to the surfaces of the samples oxidized at 800 °C in air for 300 h and in wet air for 100 h, respectively, and then platinum foils were placed on the top of the pastes as current collectors. Pt wires as electric leads were spot-welded to the sides of Pt foils. The resulting resistance of Pt wires

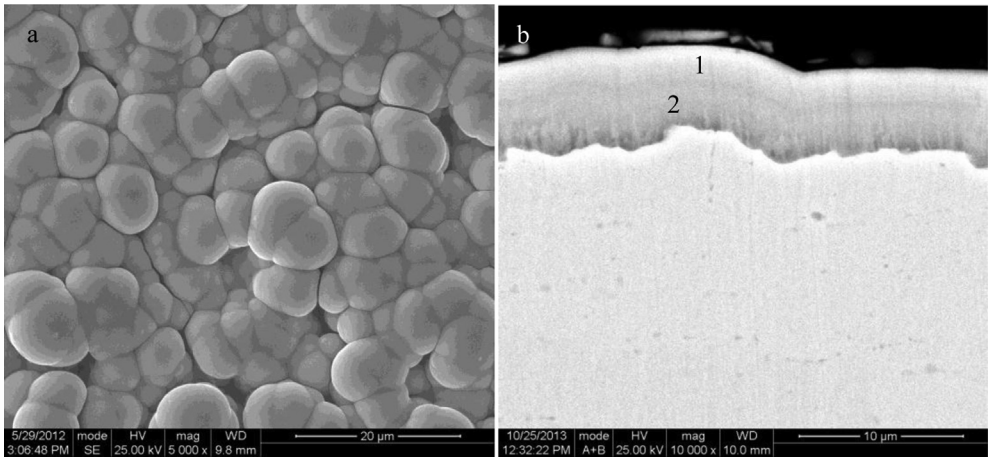

Fig. 1. Surface (a) and cross-sectional (b) morphologies of the as-deposited Co–Mn alloy layer on 430SS.

and foils were deducted from the original results. The change of ASR with temperature in air was measured.

2.4. Characterization of coatings

X-ray diffraction (XRD) using PANalytical diffractometer (X'Pertpro) with Cu ka radiation source was employed to characterize the coatings and oxidation products. The surface and cross-sections of the samples were also examined by scanning electron microscope (SEM) (FEI Inspect FSEM) equipped with an Oxford energy dispersive X-ray (EDX) microanalysis system.

3. Results and discussion

3.1. characterization of the as-prepared coatings

Fig. 1 shows the surface and cross-sectional morphologies of the as-prepared Co–Mn alloy coatings on 430SS. The coating presents a sphere-like appearance (Fig. 1a). Some crevices are observed between two spheres, probably relating to the evolution of hydrogen during electrodeposition. However, the cross-sectional observations indicate that the Co–Mn alloy layer is adherent and compact, with chemical composition of Co–22%Mn–1%Fe (atom percent) for point 1 and Co–25Mn–4%Fe–1Cr% for point 2. The ratio of Co/Mn in the Co–Mn alloy layer tends to decrease slightly with the decrease in the distance to the coating/substrate interface, probably due to the following displacement and dissolution reactions during deposition [22].

$$Co^{2+} + Mn = Co + Mn^{2+} \quad (1)$$

$$Mn + 2H^{+} = Mn^{2+} + H_2(gas) \quad (2)$$

Fig. 2 gives the XRD pattern for the Co–Mn alloy-coated 430SS annealed at 750 °C in argon for 2 h and then oxidized at 800 °C in air for 2 h. It is clear that the Co–Mn alloy layer has been converted to a $MnCo_2O_4$ spinel coating. The ratio of Co/Mn in the spinel coating is lower than that in the as-prepared Co–Mn alloy layer, suggesting that a large amount of Mn has migrated from the substrate alloy into the layer. The heat treatment in argon is aimed to eliminate the stress generated during deposition and thus promote the formation of an adhesive coating. The experimental results have confirmed that if the as-prepared Co–Mn alloy coating is oxidized directly in air, the thermally-grown Co–Mn spinel coating is prone to spallation. Fig. 3 shows the cross-sectional morphology and an EDX line scan of the as-prepared Co–Mn spinel-coated 430SS. The coating is continuous and exhibits a bi-layered microstructure composed of an external $MnCo_2O_4$ layer with a thickness of around 5 μm and a thin inner Cr-rich layer incorporated with some Mn and Co. It is also noted that some voids are present in the coatings. Theses voids mainly result from the condensation of all vacancies generated during the oxidation of the Co–Mn alloy layer.

3.2. Oxidation kinetics

Fig. 4 gives the oxidation kinetics of the uncovered and Co–Mn spinel-coated 430SS at 800 °C in air. The oxidation of 430SS follows approximately a parabolic rate law during the experimental duration of 300 h, with a rate constant of 2.91×10^{-14} g^2 cm^{-4} s^{-1}. The oxidation of the Co–Mn spinel coated 430SS obeys approximately a parabolic rate law except for the initial stage, with a rate constant of 1.59×10^{-13} g^2 cm^{-4} s^{-1}. After oxidation for 300 h, their mass gains are rather small, with a value of 0.2 mg cm^{-2} for the bare steel lower than that of 0.4 mg cm^{-2} for the coated steel.

Fig. 5 presents the mass gain curves for the oxidation of the uncoated and coated 430SS at 800 °C in wet air. Compared to the oxidation in air, the oxidation in wet air is accelerated, especially for the uncovered steel. After an incubation oxidation of around 10 h with a low mass gain 430SS suffers from a breakaway oxidation with a significantly high mass gain. This breakaway oxidation may be ascribed to that the partial failure of the protective scale formed in the incubation stage gives rise to the fast growth of non-protective Fe-rich oxide scales. Unlike the uncovered 430SS, a

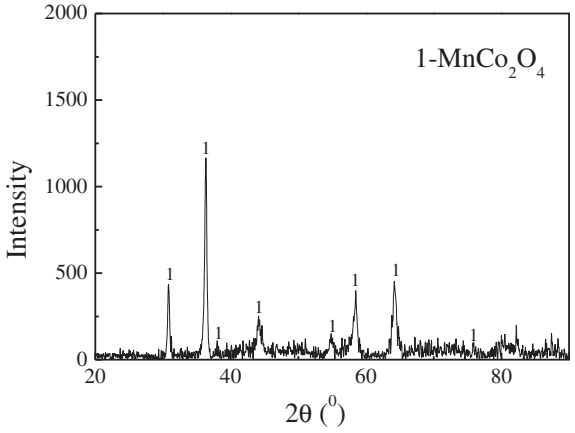

Fig. 2. XRD pattern of the as-prepared Co–Mn spinel-coated 430SS treated at 750 °C in argon for 2 h and at 800 °C in air for 2 h.

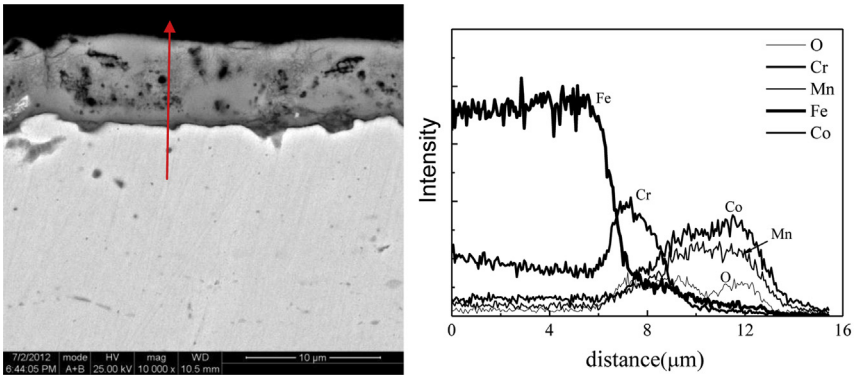

Fig. 3. Cross-sectional morphology and an EDX line scan of the as-prepared Co–Mn spinel coated 430SS.

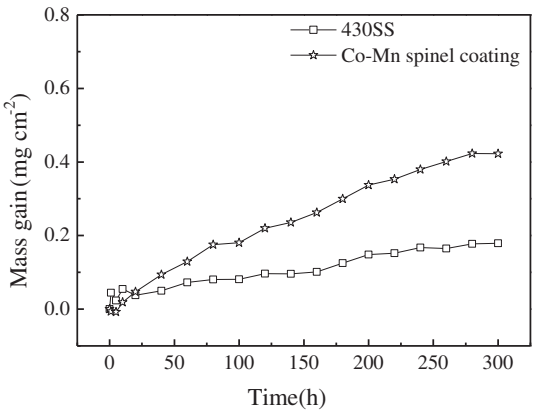

Fig. 4. Oxidation kinetics of the uncoated and Co–Mn spinel-coated 430SS at 800 °C in air.

breakaway oxidation is not observed for the coated 430SS, suggesting that the coatings can inhibit effectively the occurrence of breakaway oxidation of 430SS in wet air, and thus improve significantly its oxidation resistance.

3.3. Oxidation products

Figs. 6 and 7 give the XRD patterns of the uncovered and covered 430SS oxidized at 800 °C in air for 300 h and in wet air for 100 h, respectively. The scale formed on 430SS in air consists of $(Mn,Cr)_3O_4$ and Cr-rich $(Cr,Fe)_2O_3$, while in wet air Fe_2O_3 is also observed. The scales on the coated 430SS oxidized in both environments are still composed of $MnCo_2O_4$.

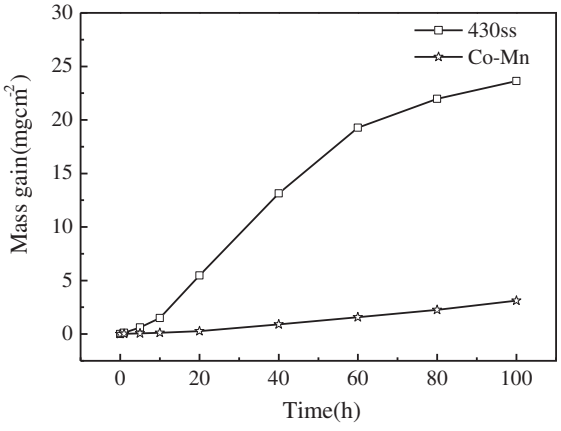

Fig. 5. Oxidation kinetics of the uncoated and Co–Mn spinel-coated 430SS at 800 °C in wet air containing 10%H_2O.

Fig. 8 shows the surface and cross-sectional morphologies of 430SS after oxidation at 800 °C in air for 300 h. Although a thin scale composed of external $(Mn,Cr)_3O_4$ and inner Cr-rich $(Cr,Fe)_2O_3$ has been formed on the alloy surface, it has a poor adhesion to the substrate. Meanwhile, a Cr-depleted layer is also formed beneath the scale.

After oxidation at 800 °C in air for 300 h, the coating still exhibits a bi-layered microstructure consisting of a thick $MnCo_2O_4$ outerlayer and a thin Cr-rich inner layer incorporated with some Mn and Co, as shown in Fig. 9. EDX analysis indicates that the chemical composition of the external spinel layer is inhomogeneous to a small extent, with a slight decrease in the ratio of Co/Mn with the decrease in the distance to the $MnCo_2O_4$ layer/Cr-rich layer interface. During oxidation, Mn in the substrate alloy may diffuse outward to contribute to the growth of oxide scales. Cr is not detected in the external part of the $MnCo_2O_4$ layer, suggesting that the Co–Mn spinel coating is effective in inhibiting the outward diffusion of Cr. Although some small voids are observed inside the $MnCo_2O_4$ layer, the coating shows a good adhesion to the substrate.

In wet air, however, in addition to a Cr-rich scale large amounts of nodules consisting of Fe oxides have been formed on the uncoated 430SS, as shown in Fig. 10. The alloy is attacked non-uniformly. In the fast corrosion regions, the alloy has formed a thick scale consisting of an external Fe oxides layer and a Fe-rich $(Fe,Cr)_2O_3$ sublayer, while in the areas corroded slightly, a thin Cr-rich $(Cr,Fe)_2O_3$ scale still exists on the alloy surface. When the initially formed Cr-rich scale goes through partial failure and a Cr-rich scale cannot re-form on the alloy surface, some Fe nodules can grow over the substrate, giving rise to the breakaway oxidation. The presence of water vapour accelerates the failure of the Cr-rich scales formed on 430SS.

Fig. 11 shows the cross-sectional morphology and an EDX line scan of the coated 430SS corroded at 800 °C in wet air for 100 h. Just as observed in air, the coating corroded in wet air still keeps the original bi-layered microstructure composed of an external $MnCo_2O_4$ layer and an inner Cr-rich layer with some Mn and Co. Cr is not detected on the surface of $MnCo_2O_4$ layer, indicating that the $MnCo_2O_4$ layer can suppress effectively the outward diffusion of Cr from the Cr-rich scale.

3.4. ASR measurements

Fig. 12 gives the change of ASR with temperature in air for the uncoated and coated 430SS oxidized at 800 °C in air for 300 h and in wet air for 100 h. ASR for all samples decreases with increasing

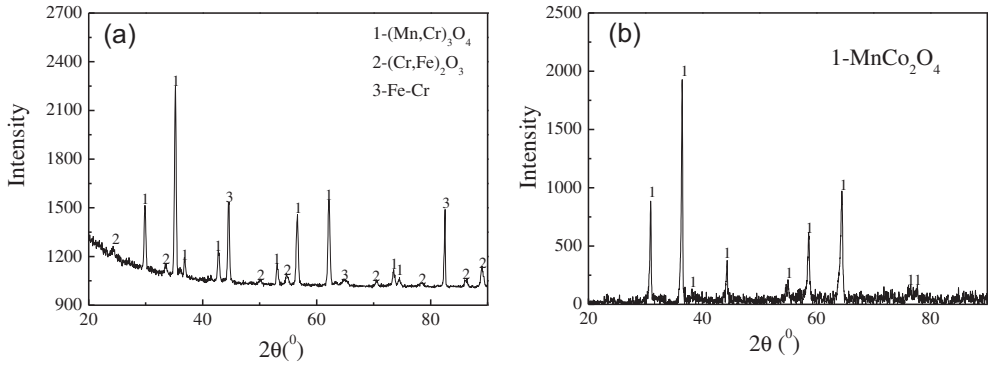

Fig. 6. XRD patterns of the uncoated (a) and Co–Mn spinel-coated (b) 430SS after oxidation at 800 °C in air for 300 h.

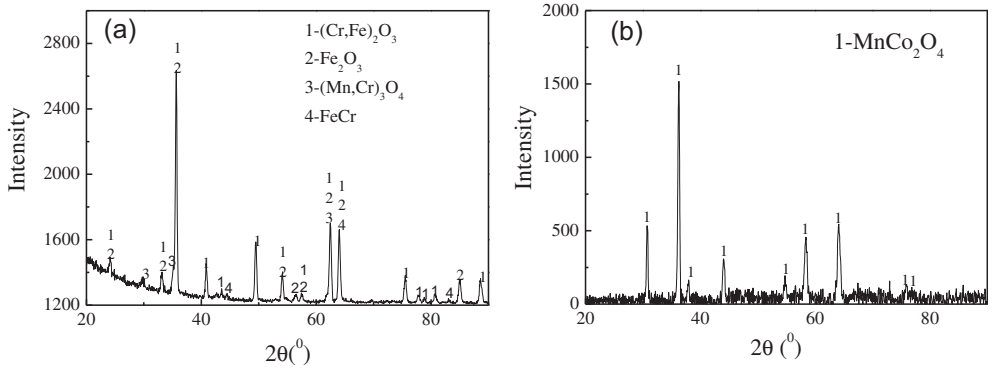

Fig. 7. XRD patterns of the uncovered (a) and Co–Mn spinel-coated 430SS (b) oxidized at 800 °C in wet air for 100 h.

temperature, suggesting that the scales exhibit the characteristic of an n-type semiconductor. ASR at 800 °C for the coated 430SS oxidized at 800 °C in air for 300 h is around 24 mΩ cm^2 obviously lower than the value of 40 mΩ cm^2 for the uncoated steel. ASR at 800 °C for the coated 430SS oxidized at 800 °C in wet air for 100 h is around 27 mΩ cm^2 significantly lower than the value of 80 mΩ cm^2 for the uncovered 430SS. It is clear that the Co–Mn spinel coatings can decrease ASR of 430SS, and the presence of 10%H_2O in air accelerates the oxidation of 430SS and thus increases its ASR.

3.5. Discussion

The oxidation of 430SS at 800 °C in air follows approximately a parabolic rate law during the experimental duration of 300 h, forming a Cr-rich scale with a poor adhesion to the substrate, while in wet air the alloy goes through breakaway oxidation after an incubation oxidation. Although the Co–Mn spinel coating has a larger mass gain in air than the uncovered 430SS, it is adherent, and can inhibit effectively the outward diffusion of Cr. Moreover, the

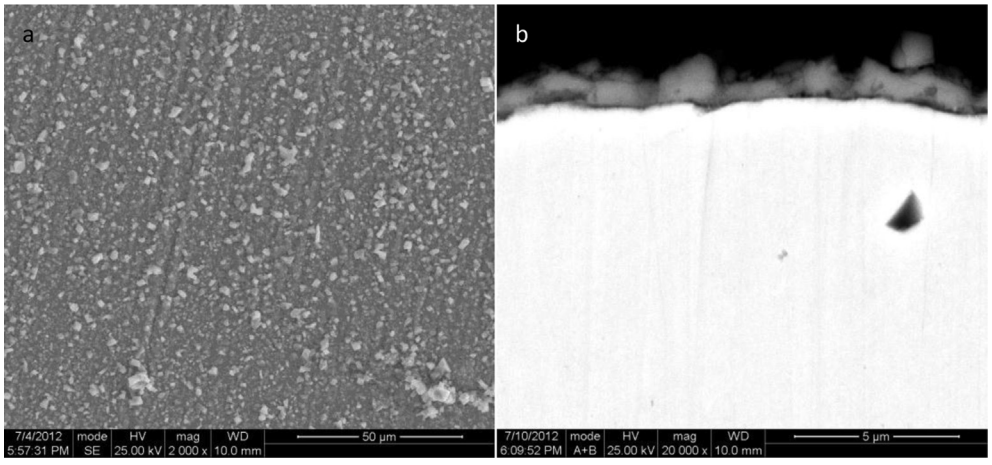

Fig. 8. Surface (a) and cross-sectional (b) morphologies of the uncovered 430SS oxidized at 800 °C in air for 300 h.

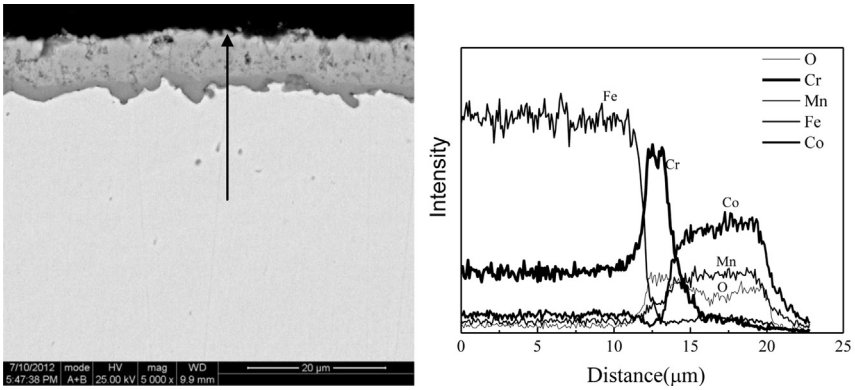

Fig. 9. Cross-sectional morphology and an EDX line scan of the Co–Mn spinel-coated 430SS after oxidation at 800 °C in air for 300 h.

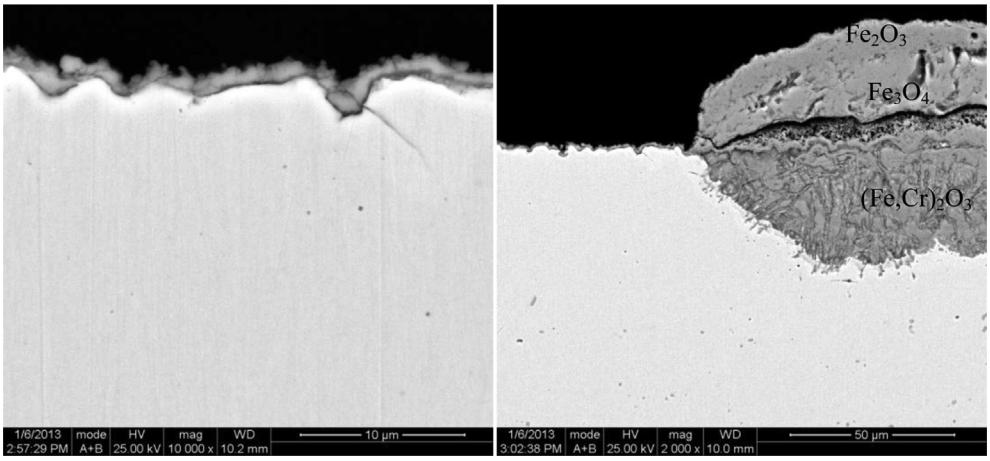

Fig. 10. Cross-sectional morphologies of the uncoated 430SS after oxidation 800 °C in wet air for 100 h.

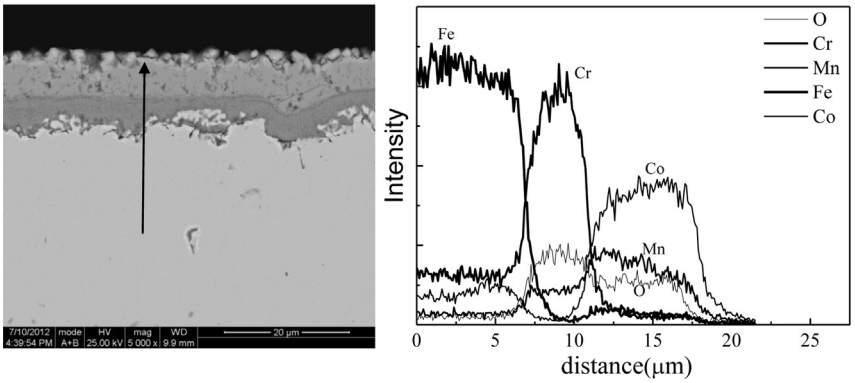

Fig. 11. Cross-sectional morphology and an EDX line scan of the Co–Mn spinel-coated 430SS after oxidation at 800 °C in wet air for 100 h.

coating stops the occurrence of breakaway oxidation of 430SS in wet air and the outward diffusion of Cr during the experimental duration of 100 h.

The presence of water vapour in air accelerates significantly the oxidation of 430SS. It has been known that water vapour increases obviously the corrosiveness of environments and increases the critical Cr content needed to form a Cr-rich scale [38,39]. The effect of water vapour on the oxidation of alloys at high temperatures has been investigated extensively. Some mechanisms, such as the change of material transport mechanisms in alloy [40], the change of defect-dependent properties of oxide scales due to the incorporation of hydrogen [41,42], and the vaporization of chromia scale from a protective Cr-rich oxide to a less protective $CrO_2(OH)_2$ [43–45] have been established to explain the accelerated corrosion induced by water vapour. Cr can be lost from the protective Cr-rich scale on 430SS exposed to wet air by the following reaction [27]:

$$Cr_2O_3(s) + 2H_2O(g) + 1.5O_2(g) \rightarrow 2CrO_2(OH)_2(g) \quad (3)$$

Cr vaporization from $MnCr_2O_4$ can be expressed by the reaction (4):

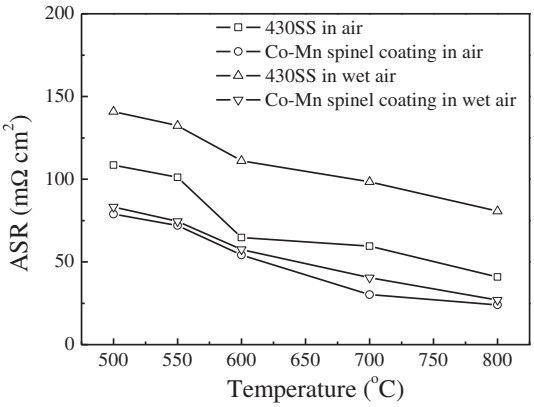

Fig. 12. ASR as a function of temperature for the uncoated and Co–Mn spinel-coated 430SS after oxidation in air for 300 h and wet air for 100 h.

$$2MnCr_2O_4(s) + \frac{5}{2}O_2(g) + 3H_2O(g) \rightarrow Mn_2CrO_4(s) + 3CrO_2(OH)_2(g) \quad (4)$$

In case the supply of Cr from the alloy to the oxide scale is insufficiently rapid to maintain a high Cr concentration in the scale, iron can diffuse easily outward to form nodules of Fe oxides. In the present study, 430SS forms a continuous Cr-rich scale beneath which a Cr-depleted zone is generated in the incubation stage with a low mass gain. However, after oxidation for a short time, the alloy goes through breakaway oxidation with a high mass gain. This accelerated oxidation is ascribed to that the initially formed Cr-rich scale on 430SS suffers from partial failure and a new Cr-rich scale cannot be re-formed due to insufficient Cr content. In fact, the low chromium content (17 wt.%) of 430SS is insufficient to maintain the growth of a protective Cr_2O_3 scale. Meanwhile, the poor adhesion of the Cr-rich scales formed on 430SS also promotes the occurrence of breakaway oxidation. The spinel coatings retard significantly the occurrence of breakaway oxidation of 430SS in wet air and inhibit the outward diffusion of Cr from the Cr-rich scale.

The spinel coatings not only improve the oxidation resistance of 430SS, but also decrease its ASR. The measured ASR includes the resistance of the scale/coating and its interface with the substrate and Pt electrode. The scale composition and thickness have a great effect on the values of ASR. ASR for the coated 430SS after oxidation in both air and wet air includes the resistance of the coating (external $MnCo_2O_4$ layer and inner Cr-rich layer incorporated with some Mn and Co) and its interface with the substrate and Pt electrode. ASR of the uncovered 430SS includes the resistance for the bi-layered scale composed of external $(Cr,Mn)_3O_4$ and inner Cr-rich $(Cr,Fe)_2O_3$, and its interface with the substrate and Pt electrode. The electrical conductivity of $MnCo_2O_4$ at 800 °C in air is around 50 S cm^{-1} which is more than three orders of magnitude higher than that of Cr_2O_3 (1×10^{-2} S cm^{-1}) and two orders of magnitude higher than that of $MnCr_2O_4$ (0.5 S cm^{-1}) [30,46,47]. Therefore, the fact that the coated steel has a significantly lower ASR than the uncovered steel is ascribed to that the coatings have a higher electrical conductivity than the oxide scales grown on 430SS. Meanwhile, the poor adhesion of the oxide scales on 430SS may also increase its interface resistance with the substrate and thus its ASR. The presence of water vapour accelerates greatly the corrosion of 430SS, giving rise to the formation of large amounts of nodules, and thus a great increase in ASR.

Garcia-Vargas et al. [20] employ atmospheric plasma spraying and wet powder spraying methods to prepare a bi-layered spinel coating composed of an external porous $MnCo_2O_4$ layer and an inner relatively dense $MnCo_2O_4$ layer. ASR for the coating is 50 mΩ cm^2 after 600 h of oxidation at 800 °C in air. Yang et al. [21] have prepared a Co–Mn spinel coating with the nominal composition of $Mn_{1.5}Co_{1.5}O_4$ by screen printing on Crofer 22 APU substrates. ASR for the spinel coated substrates is approximately 10 mΩ cm^2 after 1000 h of oxidation in air at 800 °C. Wei et al. [22] develop a $(Co,Mn)_3O_4$ spinel layer obtained by sequential electrodeposition of Mn and Co, and then by oxidation treatment on AISI-ASE 430 stainless steel substrates. ASR for the coating is rather low at 750 °C after 1500 h of oxidation, with a value of 3 mΩ cm^2. In the present investigation, ASR at 800 °C for the coated 430SS oxidized at 800 °C in air for 300 h and in wet air for 100 h is around 24 and 27 mΩ cm^2, respectively, which are significantly lower than the generally accepted upper limit of 100 mΩ cm^2 for SOFC interconnect [48]. However, the coating still exhibits higher ASR values than the spinel coatings reported in Refs. [21,22], probably due to that the coating, especially the inner Cr-rich layer is thicker.

4. Conclusions

An adhesive Co–Mn spinel coating has been prepared successfully on 430SS by galvanostatic electrodeposition of a Co–Mn alloy layer in a chlorate electrolyte suspension composed of 0.05 M $CoCl_2$, 1.25 M $MnCl_2$, 30 g L^{-1} NH_4Cl, 20 g L^{-1} NH_4Br and 0.05 M EDTA–Na_2, followed by heat treatment at 750 °C in argon, and at 800 °C in air, respectively. The coatings exhibit a bi-layered microstructure composed of an external $MnCo_2O_4$ layer and inner Cr-rich oxide layer incorporated with some Mn and Co. Although the mass gain of the coatings oxidized at 800 °C in air for 300 h is higher than that of the uncovered 430SS, the coatings show much better adhesion to the substrate than the oxide scale on 430SS. In 10%H_2O-containing air 430SS suffers from breakaway oxidation with a significantly high mass gain after a short-term incubation oxidation with a low mass gain. This kind of breakaway oxidation is related to the partial failure of the initially formed Cr-rich scale and then the growth of large amounts of Fe nodules. Applying Co–Mn spinel coatings can inhibit greatly the occurrence of breakaway oxidation of 430SS. The coatings still keep the bi-layered microstructure even after oxidation in both air and wet air. ASR at 800 °C in air for the coated steel oxidized at 800 °C in air for 300 h and in wet air for 100 h is 24 and 27 mΩ cm^2, respectively, which are lower than that for the uncovered steel. The low ASR of the coated 430SS is ascribed to that the electrical conductivity of the coatings is significantly higher than that of the oxide scales grown on the uncovered 430SS.

Acknowledgements

The project supported by National Natural Science Foundation of China, Grant No 50771101.

References

[1] B.C.H. Steele, A. Heinzel, Nature 414 (2001) 345–352.
[2] L.T. Wilkinson, J.H. Zhu, J. Electrochem. Soc. 156 (8) (2009) B905–B912.
[3] Z. Shao, W. Zhou, Z. Zhu, Prog. Mater. Sci. 83 (2011) 172–256.
[4] E. Ivers-Tiffee, W. Wersing, M. Schiebl, H. Greiner, Ber. Bunsenges. Phys. Chem. 94 (1990) 978–981.
[5] H.P. Buchkremer, U. Diekmann, L.G.J. de Haart, H. Kabs, U. Stimming, D. Stover, in: U. Stimming, S.C. Singhal, H. Tagawa, W. Lehnert (Eds.), Proc. 5th Int. Symp. Solid Oxide Fuel Cells, The Electrochemical Society, Pennington, NJ, 1997, p. 160.
[6] W.J. Quadakkers, H. Greiner, M. Hansel, A. Patlanaik, A.S. Khanna, M. Mallener, Solid State Ionics 91 (1996) 55–67.
[7] Z.G. Yang, K.S. Weil, D.M. Paxton, J.W. Stevenson, J. Electrochem. Soc. 150 (9) (2003) A1188–A1201.
[8] H. Ebrahimifar, M. Zandrahimi, Solid State Ionics 183 (1) (2011) 71–79.

[9] S. Taniguchi, M. Kadowaki, H. Kawamura, T. Yasuo, Y. Akiyama, Y. Miyake, T. Saitoh, J. Power Sources 55 (1995) 73–79.
[10] K. Hilpert, D. Das, M. Miller, D.H. Peck, R. Weib, J. Electrochem. Soc. 143 (1996) 3642–3647.
[11] S.P.S. Badwal, R. Deller, K. Foger, Y. Ramprakash, J.P. Zhang, Solid State Ionics 99 (1997) 297–310.
[12] Y.J. Xu, Z.Y. Wen, S.R. Wang, T.L. Wen, Solid State Ionics 192 (1) (2011) 561–564.
[13] W. Qu, H. Li, D.G. Ivey, J. Power Sources 138 (2004) 162–173.
[14] J.S. Yoon, J. Lee, H.J. Hwang, C.M. Whang, J.W. Moon, D.H. Kim, J. Power Sources 181 (2008) 281–286.
[15] J.J. Choi, J.H. Lee, D.S. Park, B.D. Hahn, W.H. Yoon, H.T. Lin, J. Am. Ceram. Soc. 90 (2007) 1926–1929.
[16] C. Johnson, R. Gemmen, N. Orlovskaya, Compos. Part B Eng. 35 (2004) 167–172.
[17] P. Piccardo, P. Gannon, S. Chevalier, M. Viviani, A. Barbucci, G. Caboche, R. Amendola, S. Fontana, Surf. Coat. Technol. 202 (2007) 1221–1225.
[18] P. Gannon, M. Deibert, P. White, R. Smith, H. Chen, W. Priyantha, J. Licas, V. Gorokhousky, Int. J. Hydrogen Energy 33 (2008) 3991–4000.
[19] B. Hua, J.A. Pu, W. Gong, J.F. Zhang, F.S. Lu, L. Jian, J. Power Sources 185 (2008) 419–422.
[20] M.J. Garcia-Vargas, M. Zahid, F. Tietz, A. Aslanides, ECS Trans. 7 (2007) 2399–2405.
[21] Z.G. Yang, G.G. Xia, S.P. Simner, J.W. Stevenson, J. Electrochem. Soc. 152 (2005) A1896–A1901.
[22] P. Wei, X. Deng, M.R. Bateni, A. Petric, Corrosion 63 (2007) 529–536.
[23] N. Shaigan, D.C. Ivey, W.X. Chen, J. Power Sources 185 (2008) 331–337.
[24] N. Shaigan, D.C. Ivey, W.X. Chen, J. Power Sources 183 (2008) 651–659.
[25] N. Shaigan, W. Qu, D.G. Ivey, W.X. Chen, J. Power Sources 195 (2010) 1529–1542.
[26] J.W. Wu, X.B. Liu, J. Mater. Sci. Technol. 26 (4) (2010) 293–305.
[27] K. Hilpert, D. Das, M. Miller, D.P. Peck, R. Wei, J. Electrochem. Soc. 143 (1996) 3624–3647.
[28] C. Gindorf, L. Singheiser, K. Hilpert, Steel Res. 72 (2001) 528–533.
[29] X. Chen, P.Y. Hou, C.P. Jacobson, S.J. Viso, L.C. De Jonhe, Solid State Ionics 176 (2005) 425–433.
[30] Z.G. Yang, G.G. Xia, X.H. Li, J.W. Stevenson, Int. J. Hydrogen Energy 32 (2007) 3648–3654.
[31] M.R. Bateni, P. Wei, X.H. Deng, A. Petric, Surf. Coat. Technol. 201 (2007) 4677–4684.
[32] W.F. Wei, W.X. Chen, D.G. Ivey, J. Power Sources 186 (2009) 428–434.
[33] J.W. Wu, Y.L. Jiang, C. Johnson, X.B. Liu, J. Power Sources 177 (2) (2008) 376–385.
[34] J.W. Wu, C.D. Johnson, Y.L. Jiang, R.S. Gemmen, X.B. Liu, Electrochim. Acta 54 (2) (2008) 793–800.
[35] Q.F. Wei, X.L. Ren, J. Du, S.J. Wei, S.R. Hu, Miner. Eng. 23 (7) (2010) 578–586.
[36] O.E. Kongstein, G.M. Haarberg, J. Thonstad, J. Appl. Electrochem. 37 (2007) 669–674.
[37] Z.J. Feng, C.L. Zeng, J. Power Sources 1995 (2010) 7373–7374.
[38] P. Kofstad, High Temperature Corrosion, Elsevier Applied Science Publishers Ltd, London and New York, 1988.
[39] C.T. Fujii, R.A. Meussner, J. Electrochem. Soc. 111 (1964) 1215.
[40] M. Thiele, H. Teichmann, W. Schwarz, W.J. Quadakkers, VGB Kraftwerkstech. 77 (1997) 129.
[41] G. Hultquist, B. Tveten, E. Hornlund, M. Limback, R. Haugsrud, Oxid. Met. 56 (2001) 313.
[42] G. Hultquist, B. Tveten, E. Hornlund, Oxid. Met. 54 (2000) 1.
[43] H. Asteman, K. Segerdahl, J.E. Svensson, L.G. Johansson, Mater. Sci. Forum 369–372 (2001) 277.
[44] F. Liu, J.E. Tang, T. Jonsson, S. Canovic, K. Segerdahl, J.E. Svensson, M. Halvarsson, Oxid. Met. 66 (2006) 295.
[45] D.J. Young, High Temperature Oxidation and Corrosion of Metals, Elsevier, Oxford, 2008, pp. 455–495.
[46] K. Wang, Y. Liu, J.W. Fergus, J. Am. Ceram. Soc. 94 (12) (2011) 4490–4495.
[47] M.K. Mahapatra, K. Lu, X.B. Lu, J.W. Wu, Int. J. Hydrogen Energy 35 (15) (2010) 7945–7956.
[48] W.Z. Zhu, S.C. Deevi, Mater. Sci. Eng. A348 (2003) 227–243.